Reducing the L-H Transition Power Threshold via Edge Rotation Reversals and Increased Triangularity

L. Schmitz,[1] Z. Yan[2], T.L. Rhodes,[1] L. Zeng,[1] G.R. McKee,[2] P.Gohil,[3] C.C. Petty[3]

[1]*University of California Los Angeles, PO Box 957099, Los Angeles, CA 90095-7099, USA*
[2]*University of Wisconsin-Madison, 1500 Engineering Dr., Madison, WI 53706, USA*
[3]*General Atomics, PO Box 85608, San Diego, CA 92186-5608, USA*

In this paper we demonstrate that edge toroidal rotation changes dynamically across the L-H transition, and that a rapid local rotation reduction or reversal can reduce the L-H transition power threshold P_{LH} significantly. Understanding of the role of toroidal rotation is very important for H-mode access, as the magnitude of intrinsic L-mode edge rotation in ITER is unknown. It is also shown that minor plasma shape changes (here, a small increase in lower triangularity) can reduce P_{LH}. Minimizing P_{LH} is crucial for ITER and future burning plasma experiments, in particular for the planned ITER PFPO-1 operation in hydrogen [1], where the available ECH power is moderate (20-30 MW).

Figure 1 shows the observed L-H power threshold P_{LH}, normalized to the threshold predicted by the 2008 ITPA (Martin) scaling [2]

$$P_{LH-08}[MW] = 0.049 n[10^{20} m^{-3}]^{0.72} B[T]^{0.8} S[m^2]^{0.96} * 2 / A_i \qquad [1]$$

versus $\Delta v_{\boldsymbol{E}\times\boldsymbol{B}}$, the differential in $\boldsymbol{E}\times\boldsymbol{B}$ velocity across the outer shear layer (OSL, ρ =0.96-1.0, at/just inside the last closed flux surface). Here, S is the plasma surface area, and the mass number A_i has been incorporated to account for the isotope threshold dependence [3]. The data was obtained in ITER-Similar-Shape (ISS) lower single null hydrogen plasmas in DIII-D, for plasma parameters $<n_e>$ ~3.3×10^{19} m^{-3}, B=2.05 T, I_p =1 MA, q_{95}=5.1. P_{LH}/P_{LH-08} is observed to increase when the $\boldsymbol{E}\times\boldsymbol{B}$ velocity shear in the outer shear layer is reduced, and can be substantially higher than predicted by the 2008 (Martin) scaling. The $\boldsymbol{E}\times\boldsymbol{B}$ velocity is measured here via Doppler Backscattering (DBS) [4]. TGLF stability calculations, used to estimate the turbulence phase velocity, indicate an offset of ~0.7-1 km/s in the electron diamagnetic direction, fairly independent of radius, in the OSL, hence $\Delta v_{\boldsymbol{E}\times\boldsymbol{B}}$ can be directly extracted from the measured DBS Doppler shift, using GENRAY ray tracing to determine the probed DBS wavenumber

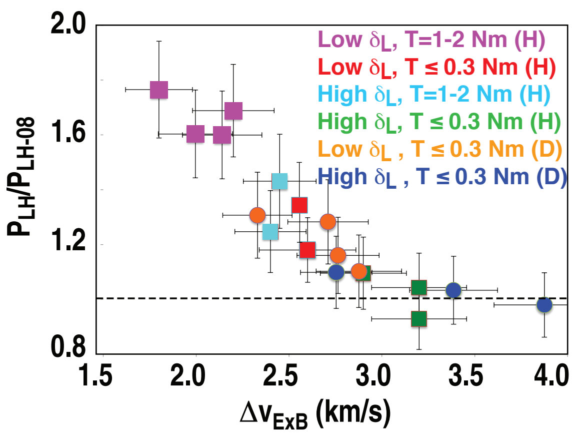

Fig. 1: P_{LH}/P_{LH-08} vs. $\boldsymbol{E}\times\boldsymbol{B}$ shear in the outer shear layer (ω_{ExB} =$\Delta v_{E\times B}/dr$ with dr ~0.7 cm)) for high and low triangularity H and D plasmas.

and backscattering radius. The pronounced dependence of P_{LH} on NBI torque is immediately obvious in Fig. 1, as also observed earlier in DIII-D [5]. A slight increase in lower triangularity (from $\delta_L \sim 0.72$ to $\delta_L \sim 0.82$) reduces the power threshold by ~5-10% (for more detail see also Figure 4 below).

Previous experiments in DIII-D, ASDEX-U, and C-MOD have shown that the L-H power threshold is substantially increased with unfavorable ion ∇B drift direction (away from the active divertor) [6-8]. This effect has been attributed to differences in the radial flow boundary condition that arise mainly due to transport-driven parallel flows in the scrape-off layer [due to enhanced (ballooning) plasma loss around the outboard midplane]. These parallel flows are directed preferentially to either the outboard or inboard divertor target depending on ion ∇B drift direction [8]. The parallel flow includes both Pfirsch-Schlueter and transport-driven components. In addition, significant differences in turbulence advection velocity and a reduction of the turbulent Reynolds stress have been observed in plasmas with unfavorable ion ∇B drift direction approaching the L-H transition [9,10].

Figure 2 shows the time evolution of the plasma density, toroidal edge rotation, and edge electron temperature across the L-H transition in a lower single null (LSN) diverted deuterium plasma (B_t =1.95 T, I_p=-1.4 MA, q_{95}=3.6). Here, the ion ∇B drift was directed away from the active (lower single-null) divertor (unfavorable ∇B drift direction). The plasmas compared here employed either balanced neutral beam injection (in black; P_{LH} =1.65 MW) or moderate co-current NBI torque (in red, P_{LH} =2.15 MW) or counter-current torque (in blue, P_{LH} =1.4 MW). The L-H power threshold is lowest for counter-current injection, and highest for co-current injection. The neutral beam power shown here is the decisive contribution to P_{LH}; Ohmic power (~600 kW), core radiated power (~250 kW) and dW_{dia}/dt (~600 kW) are similar for the three discharges. Considering the radial ion force balance

$$E_r = \frac{1}{ne}\nabla p_i + v_\phi B_\theta - v_\theta B_\phi$$

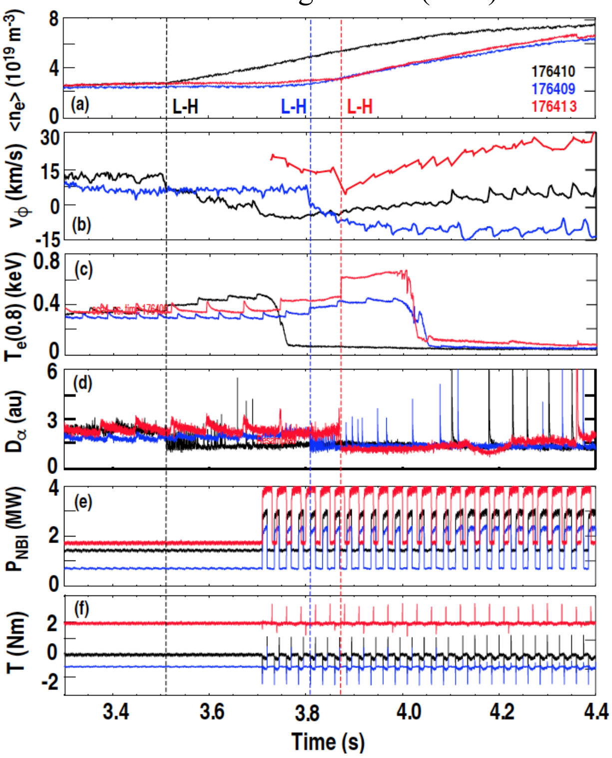

Fig. 2: Evolution of (a) plasma density; (b) toroidal Carbon rotation velocity at ρ ~ 0.78; (c) electron temperature at ρ =0.8; (d) D_α signal; (e) neutral beam power; (f) neutral beam torque across the L-H transition for co-, counter-, and balanced NBI.

E_r will become more positive in the edge when the $v_\phi B_\theta$ term in the force balance is positive (corresponding to co-rotation in DIII-D), counteracting the (negative) diamagnetic (pressure gradient) term in the force balance, and reducing edge ***E***×***B*** shear. In contrast, E_r in the edge will become more negative when counter-current toroidal rotation is driven, increasing local ***E***×***B*** shear. Fig. 2(b) shows a rapid reduction (or reversal) in the edge toroidal impurity (carbon) rotation preceding the L-H transition. While main ion (deuterium) toroidal rotation may differ from carbon rotation, as discussed in more detail elsewhere [11], the observed rotation reduction or reversal is consistent with increased shear in the edge ***E***×***B*** velocity measured by DBS, resulting in a reduced power threshold not far above the threshold observed in LSN plasmas with favorable ion ∇*B* drift direction [Fig. 3(a)]. The rapid rotation transitions [Fig. 2(b)] are localized near ρ ~0.94. Fig. 2(c) shows the electron temperature measured by Electron Cyclotron Emission (ECE) at ρ ~0.8, and demonstrates that the rotation reduction/reversals appear to be triggered by sawtooth crashes and the concomitant transient increase in edge power flow (the loss of the ECE signal after the L-H transition indicates cutoff (the local cutoff frequency exceeds the 2nd cyclotron harmonic emission frequency).

Figure 3(a) shows the L-H transition power threshold as function of applied NBI torque for deuterium plasmas with unfavorable and favorable ion ∇*B* drift direction. P_{LH} is typically increased by ~ 50-80% with unfavorable ion grad ∇*B* drift direction, however toroidal rotation transitions significantly reduce P_{LH} over a range in NBI torque, but most effectively for balanced torque or with low counter-I_p torque. Fig. 3(b) shows radial profiles of toroidal (carbon) edge rotation, for different times approaching the L-H transition, and shortly afterwards. The rotation reduction/ reversal commences locally near ρ ~ 0.94; the layer of reduced rotation then expands radially over several ms, providing increased ***E***×***B*** flow shear to induce the L-H transition. Fig. 3(c) shows that the power threshold increases linearly with the toroidal rotation minimum

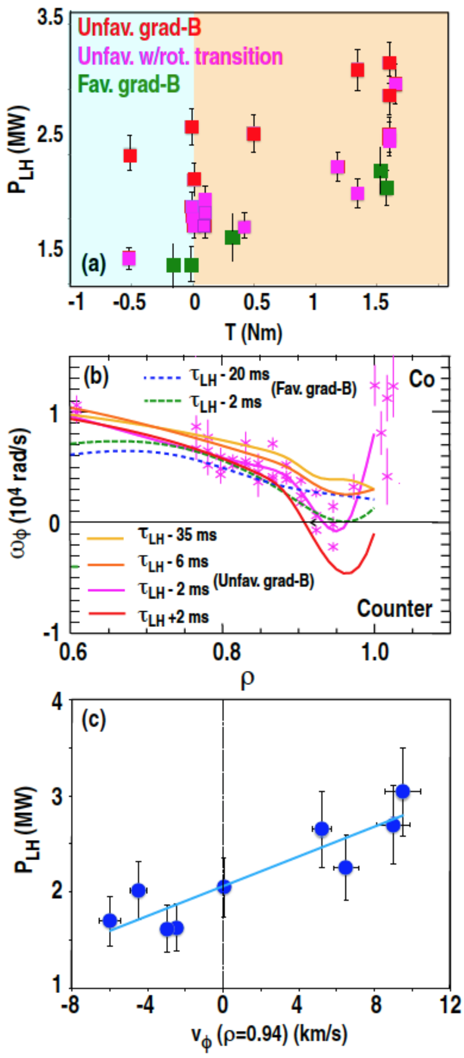

Fig. 3: (a) L-H power threshold for favorable and unfavorable ion ∇B drift direction vs. NBI torque; (b) radial profile of toroidal rotation near the L-H transition (fav. and unfav. ∇B); (c) P_{LH} vs. *toroidal rotation minimum at ρ ~0.94.*

at ρ~0.94. $\boldsymbol{E}\times\boldsymbol{B}$ shear is increased inboard and outboard of the rotation minimum, triggering the L-H transition at lower threshold power. However, the increase of the rotation minimum with NBI torque requires an increasing contribution of the (negative) pressure gradient term to provide sufficient shear to trigger the transition at high NBI torque, hence the threshold increases with T_{NBI}. Rotation reversals have been observed at different densities, down to the lowest achievable edge ion collisionality in DIII-D. If edge rotation reversals can be triggered via localized ECH power deposition in the edge plasma, the power threshold could potentially be lowered via locally increased $\boldsymbol{E}\times\boldsymbol{B}$ shear, however this approach would only be successful if the additional thermal electron loss power due to ECH is moderate (less than the achieved power threshold reduction).

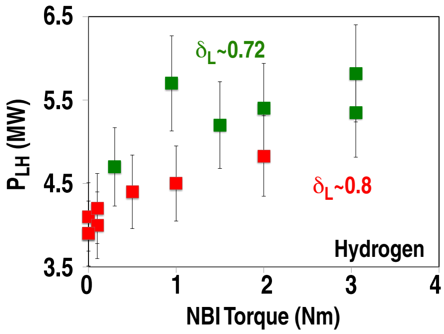

Fig. 5: L-H transition power threshold vs. neutral beam torque for two different values of the lower tringularity δ_L.

In ISS hydrogen and deuterium plasmas (with favorable grad-$\boldsymbol{B}$ drift direction), a slight (~12%) increase in lower triangularity (from δ_{L}= 0.72 in ISS shape to δ_{L}=0.8) results in a clear reduction in L-H power threshold (shown in figure 4 vs. NBI torque for hydrogen plasmas). As shown above in Fig. 1, $\boldsymbol{E}\times\boldsymbol{B}$ shear flow in the outer shear layer increases at higher triangularity δ_{L}, and the normalized power threshold $P_{\mathrm{LH}}/P_{\mathrm{LH\text{-}08}}$ decreases clearly with increasing δ_{L}. At higher triangularity and approximately balanced torque ($T \leq 0.3$ Nm), $\boldsymbol{E}\times\boldsymbol{B}$ shear in the OSL is maximized, and $P_{\mathrm{LH}} \sim P_{\mathrm{LH\text{-}08}}$ has been found in both H and D plasmas for the edge safety factor employed here (q_{95} =5.1); with $\mathrm{P_{LH\text{-}08}(H) = 2\times P_{LH\text{-}08}(D)}$ (see equation [1]). Recent DIII-D hydrogen experiments with q_{95}=3.6 in electron-heat-dominated plasmas have however shown a higher power threshold due to increased electron loss power [12].

This material is based upon work supported by the U.S. Department of Energy, Office of Science, Office of Fusion Energy Sciences, using the DIII-D National Fusion Facility, a DOE Office of Science user facility, under Awards DE-FG02-08ER54984, DE-FG02-08ER 54999, DE-AC05-00OR22725, and DE-FC02-04ER54698.

[1] ITER Organization ITER research plan within the staged approach *ITER Technical Report* ITR-18-003 (2018) pp. 57 164. (www.iter.org/technical-reports)

[2] Martin Y.R., Takizuka T. et al. 2008 *J. Physics: Conf. Series* 123 012033.

[3] Righi E. et al. 1999 *Nucl. Fusion* 39 309.

[4] Hillesheim J.C., Peebles W.A., Rhodes T.L., Schmitz L. et al 2010 *Rev. Sci. Instr.* **81** 10D907

[5] McKee, G.R., Gohil P., Schlossberg D.J. et al. 2009 *Nucl. Fusion* **49** 115016

[6] Gohil P., Jernigan T.C., Osborne T.H. et al. 2010 *Nucl. Fusion* **50** 064011

[7] Snipes, J.A., et al., 1996 *Nucl. Fusion* **36** 1217

[8] LaBombard B., Rice J., Hubbard A.E., Hughes J.W. et al. 2005 *Phys. Plasmas* **12** 056111

[9] Fenzi C., McKee G.R., Fonck R.J., Burrell K.H. et al., 2005 *Phys. Plasmas* **12** 062307

[10] Yan Z., McKee. G.R., Kriete D.M., Schmitz L. et al., 28th IAEA FEC conference, May 10-15, 2021

[11] Haskey, S.R., Grierson, B.A., Chrystal, C., Ashourvan, A. et al. 2018 *Plasma Phys. Control. Fusion* **60** 105101

[12] Schmitz L., Wilcox R.S., Shiraki D., Rhodes T.L. et al. 28th IAEA FEC conference, May 10-15 2021